IEEE Robotics and Automation Letters (RAL) paper presented at the
2020 IEEE International Conference on Robotics and Automation (ICRA)
31 May - 31 August, 2020. Paris, France

Mechanical Shock Propagation Reduction in Robot Legs

B. Roodra P. Singh[1,2] Roy Featherstone[1]

Abstract— **This paper shows how the mass distribution in a robot's leg affects the propagation of mechanical shocks from the foot to the torso. An example is given of a leg design that propagates no shock at all; and a formula is given for the propagation of shock in a general robot leg, modelled as a chain of rigid bodies, assuming that the foot makes a point or small-area contact when it strikes the ground.**

I. Introduction

Mechanical shocks arise in legged robots whenever a foot strikes a supporting surface. These shocks can propagate up the leg and into the torso, where they can have a variety of undesirable effects such as saturating accelerometers, shaking loose screws and electrical connectors, blurring camera images, and so on. It is therefore a good idea to try to minimize the magnitudes of shocks reaching the torso. Two obvious ways to do this are soft feet and velocity matching of the foot to the ground before landing. This paper considers a third possibility, which is to design the mass distribution within the leg so as to reduce the transmission of shocks from the foot to the torso. If the mass distribution satisfies certain criteria then the transmission of shocks can be reduced all the way to zero.

The point of this paper is that there is often some freedom to choose where to place the parts in a robot leg design, which affects the overall mass distribution within the leg. So there is a possibility to exploit this freedom to reduce shock propagation. This gives the designer one more tool to use in addition to techniques such as springs and soft feet.

Specifically, this paper considers the following problem. Given a robot leg modelled as a chain of rigid bodies, which is in a known configuration at the moment the foot strikes the ground, what is the relationship between a step change in the velocity of the foot and the corresponding step change in the velocity of a chosen point in the torso, and how is this relationship affected by the mass distribution within the leg? It is assumed that the step change in the foot's velocity is caused by a ground-reaction impulse, and that some fraction of this impulse is propagated up the leg, eventually reaching the torso. It is also assumed that the foot hits the ground at a single point, or an area small enough that it can be approximated with a single point located at the centre of pressure.

The paper is organized as follows. First, previous works on shock reduction are reviewed; then a little background theory is presented; then a design for a simple three-link leg is presented in which the transmission from the foot to the upper leg of any shock caused by a ground-reaction impulse lying in the plane of the leg is exactly zero. Finally, a general formula is given for the matrix that maps a step change in velocity of a point P in the foot to the corresponding step change in velocity of a point Q in the torso, where P is the point where the foot strikes the ground. This matrix provides a measure of shock propagation that could be used to optimize the leg's design parameters.

[1]Dept. Advanced Robotics, Istituto Italiano di Tecnologia, Genoa, Italy
[2]Dept. Information Engineering, University of Pisa, Italy

II. Previous Works

One of the simplest ways to cushion the torso from impacts at the feet is to use a spring. Raibert's original hopping robots [20] used the compressibility of air in their pneumatic pistons as a spring, mainly to recycle energy from one hop to the next, but it also had the side-effect of protecting the torso from shock. Alexander [1] proposed the use of springs as foot pads to absorb shocks when the foot of a legged robot experiences large impact forces. The reasoning in [1] to use padded feet in robots was biologically inspired from the padded paws of mammals.

As robots became heavier and faster, the need to absorb the large impact forces and prevent them from propagating up the leg and into torso of the robot gained further attention for legged robots such as bipeds. In [26], an intricate foot mechanism was developed to aid a biped robot in locomotion through absorption of impact forces using a shock-absorbing foam; while [18] proposed to actively control damping in the leg of a biped robot, in order to reduce the magnitude of the impacts during locomotion.

Impact force reduction strategies for bipeds and quadrupeds gained attention in robot leg/foot design in the last two decades; for example, a biped with flexible feet in [4], use of a soft-landing trajectory with an optimal velocity for a planar hopping robot in [22], optimized leg motion trajectories for a hexapod in [21], and a comparison of different types of foot designs for humanoid robots in [17]. Another foot mechanism is proposed in [14] to measure impact forces using force-sensing resistors, which then leads to a passivity-based control. A common reasoning for shock reduction can be noticed in [4], [14], [16], [17], [18], [21], [22], [26], which is to prevent the impact forces from propagating to the robot's leg and torso where they might damage the robot's components or make it unstable and degrade its locomotion performance.

In the last decade, in addition to using the direct method of having soft feet and active impedance regulation, some other shock reduction strategies, sometimes in combination with these two, have been proposed. One of these is the terrain

adaptive controller in [11] that changes the gains and structure of the controller based on readings from a force sensor at the foot. A bio-inspired method in [15] bases the design of a biped robot foot on the flexibility of the human foot with toes and heels. Several other techniques that aim to reduce impact forces have been proposed, such as optimizing robot leg configuration, where a bent leg is advantageous in reducing the impact forces [25], reinforcement-learning-based active impedance control [6], model-based passive compliance using configuration-dependent stiffness and damping of the robot [5], calculating change in joint velocities resulting from impulsive forces using robot configuration for grasping applications in [24], using a specific pose and joint stiffness on landing that reduces impact forces [3] for planar robots, employing artificial muscles and a magnetorheological brake [13], and biologically inspired soft material based foot pad designs to enhance friction and strong damping in [12]. Another recent work [23] has focused on different materials for foot design to choose a particular trade-off between stiffness and damping that enables energy-efficient foot design along with reduced impact forces. All is not perfect with a springy foot though: [19] shows that a spring-loaded foot can cause rebound behavior, while for active control methods the amount of time required for active impedance regulation to kick in may make it unsuitable for absorbing peak impacts.

III. Background Theory

An introduction to impulsive dynamics can be found in [10], and a brief treatment in [9]. Impulse is defined to be the time integral of force. However, we are concerned with a special kind of impulse, which is the limit as $\Delta t \to 0$ of a force $f/\Delta t$ acting over an interval Δt. Such impulses arise when rigid bodies collide, and they cause step changes in velocity. If a rigid body having inertia $\boldsymbol{I}$ is subjected to an impulse $\boldsymbol{\iota}$ then the resulting change in velocity, $\Delta\boldsymbol{v}$, is given by the impulsive equation of motion

$$\boldsymbol{\iota} = \boldsymbol{I}\Delta\boldsymbol{v}\,, \tag{1}$$

where $\boldsymbol{\iota}$ and $\Delta\boldsymbol{v}$ are spatial (6D) vectors, and $\boldsymbol{I}$ is a spatial inertia (a 6×6 matrix) [9]. If the body is connected to another body via a joint then the response changes, and the equation becomes

$$\boldsymbol{\iota} - \boldsymbol{\iota}_{\mathrm{J}} = \boldsymbol{I}\Delta\boldsymbol{v}\,,$$

where $\boldsymbol{\iota}_{\mathrm{J}}$ is the impulse transmitted through the joint to the other body. Given the inertias of the two bodies and the kinematics of the joint, it is possible to express $\boldsymbol{\iota}_{\mathrm{J}}$ as a function of $\boldsymbol{\iota}$, and hence to eliminate it from this equation, resulting in

$$\boldsymbol{\iota} = \boldsymbol{I}^A\Delta\boldsymbol{v}\,, \tag{2}$$

where $\boldsymbol{I}^A$ is the body's *articulated-body* inertia [9], which is the inertia that it appears to have given that it is connected to another body via a joint.

In this paper we assume that an impulse arising from a collision can be characterized by its magnitude and line of action. This assumption is valid if the bodies collide at a single point or over an area small enough that it can reasonably be approximated with a point located at the centre of pressure. The line of action passes through the point of contact, and lies inside or on the friction cone.

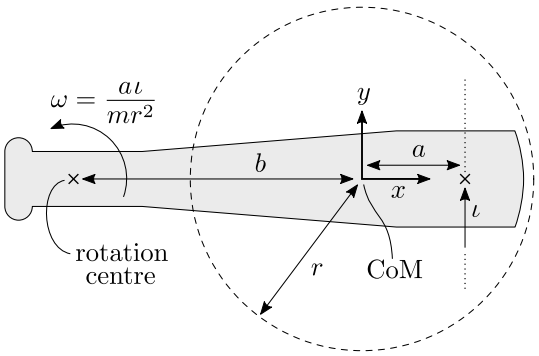

Fig. 1. The relationship between the line of action of an impulse acting on a rigid body and the rotation centre of the velocity it causes.

As this paper is concerned only with *step changes* in velocity, rather than absolute values, from here on we shall drop the delta from $\Delta\boldsymbol{v}$, and use the term 'velocity' to mean 'step change in velocity'.

A. The Planar Special Case

A basic result of planar kinematics is that a rigid body's velocity at any instant is either a pure translation or a rotation about a point somewhere in the plane, which is called the (instantaneous) rotation centre. If an impulse acts on a rigid body then it produces a pure translation if its line of action passes through the body's centre of mass (CoM), and a pure rotation otherwise. In the latter case, there is a simple geometrical relationship between the line of action and the position of the rotation centre.

Referring to Figure 1, suppose that a rigid body receives an impulse of (signed) magnitude ι acting along a line that misses the body's CoM by a distance a. We can place a coordinate frame with its origin at the CoM and y axis parallel to the line of action, so that the line passes through the point $(a, 0)$ on the x axis. Let the body have a mass m and a radius of gyration r, so that its rotational inertia about its CoM is mr^2. The effect of the impulse can now be calculated as follows. First, the given impulse can be expressed as the sum of an impulse of magnitude ι acting along the y axis and an impulsive couple of magnitude $a\iota$, which is the moment of the given impulse about the origin. The former produces a translational velocity of magnitude $v = \iota/m$, and the latter produces a rotation about the CoM of magnitude $\omega = a\iota/(mr^2)$. The effect of the given impulse is the sum of these two velocities, which is a rotation of magnitude ω about the point $(-b, 0)$, where b is given by the formula

$$ab = r^2\,. \tag{3}$$

This result can be verified by observing that a rotation of magnitude ω about $(-b, 0)$ causes the CoM to translate in the y direction with magnitude $\omega b = \iota/m$. Note that neither m nor ι appears in (3).

If the body happens to be a cricket or baseball bat, or similar object, and its handle is located at $(-b, 0)$, then the point $(a, 0)$ is called the *centre of percussion*, or, more colloquially, the 'sweet spot' [2]. It has the following special property: if a ball strikes the bat along any trajectory that passes through the centre of percussion at right angles to the x axis, then the batsman feels no jarring of his hands (i.e., no mechanical shock) because the effect of the impact is a pure rotation about the handle.

Now suppose that the body in Figure 1 is connected to a second body via an unactuated revolute joint located at $(-b, 0)$. In this case, no impulse is transmitted through the bearings, because the velocity caused by the impulse is a rotation about this point, and so no shock is passed on to the second body.

Now suppose, in addition, that the direction of the impulse can vary, although the line of action still passes through $(a, 0)$; and suppose also that the second body has the property that an impulse acting on this body along the x axis causes the body-fixed point at $(-b, 0)$ to move in the same direction as the impulse. In this case, the impulse acting on the first body can be regarded as the sum of an impulse of magnitude ι_x acting along the x axis and an impulse of magnitude ι_y acting along the original line of action. The result is that ι_y causes only a rotation of the first body about $(-b, 0)$, while ι_x causes both a pure translation of the first body in the x direction and an impulse in the x direction transmitted from the first to the second body.

So we have a situation in which both components of the original impulse have an effect on the first body, but only one has an effect on the second. The other component has been prevented from propagating across the joint, and this has been achieved simply by requiring that the line of action passes through $(a, 0)$ and the joint is located at $(-b, 0)$. This idea can be extended to a third body and second joint, which is the subject of the next section.

In the above, we assumed that the joint is unactuated, but this is unnecessarily restrictive. All that we really require is that there is no impulse in the direction of motion allowed by the joint. So the joint could have passive elements such as springs and dampers, and it could be actuated by any type of actuator that does not generate an impulse in response to a received impulse on one of the bodies. Actuators with this property include direct-drive motors and any actuator with a series elastic element. Harmonic drives may or may not qualify as series elastic elements for the purposes of calculating impulsive dynamics, depending on how stiff they are. The test is this: does the output force of the harmonic drive change during the course of the impact event by an amount that is significant compared with the impact forces? If the answer is 'no' then it can be regarded as a series elastic element.

IV. An Ideal Leg Design

For mammals and birds, and robots that resemble them, legged locomotion is a mostly planar activity. Therefore, a planar rigid-body model of such a robot is useful because it can describe most of the motion that takes place, and most of the forces that arise. This section presents a planar model of a three-link leg, shown in Figure 2, which has the property that the propagation of shock from the foot towards the torso stops at the knee. In a 3D robot equipped with this leg, only the out-of-plane component of shock would be felt above the knee.

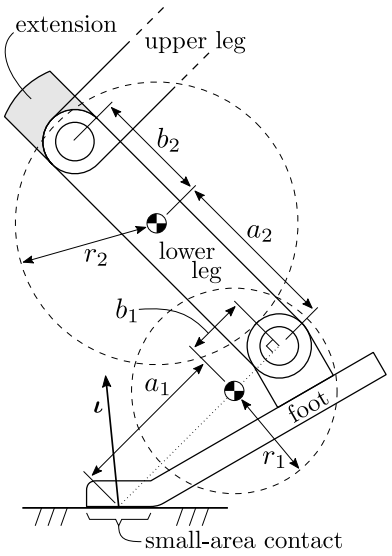

Fig. 2. A 3-link planar leg with zero transmission of shocks from the contact point (or centre of pressure) in the foot to the upper leg.

The design consists of a foot, lower leg and upper leg connected together via revolute joints at the ankle and knee. It is assumed that the actuators driving these joints do not generate impulses of their own, as explained in the previous section. The important attributes of this design are the six lengths a_i, b_i and r_i, $i = 1, 2$, and the angle at the ankle at the moment of impact, which must be $90°$. The lengths must satisfy $a_i b_i = r_i^2$, as in (3).

This leg works as follows. First, the ground-reaction impulse, $\boldsymbol{\iota}$, can be decomposed into a component $\boldsymbol{\iota}_x$ along the line from the contact point to the ankle, and a component $\boldsymbol{\iota}_y$ perpendicular to it. The former causes a translational velocity of the foot in the direction of the impulse, while the latter causes a rotation of the foot about the ankle. Thus, some fraction of $\boldsymbol{\iota}_x$ is propagated from the foot to the lower leg, but $\boldsymbol{\iota}_y$ affects only the foot, as explained in the previous section. Now, the impulse received by the lower leg is perpendicular to the line between the two joints, and the ankle is located at the lower leg's centre of percussion, if the knee is regarded as the handle, so this impulse causes only a pure rotation of the lower leg about the knee joint, and therefore does not propagate past the knee.

Viewed in terms of cricket or baseball bats, this design is two bats at right angles, each one blocking one component of the ground-reaction impulse, so that no part of the impulse reaches the upper leg. Clearly, this idea also works for a two-link leg, such as is common in robot quadrupeds, in which case the foot, lower leg and upper leg become the lower leg,

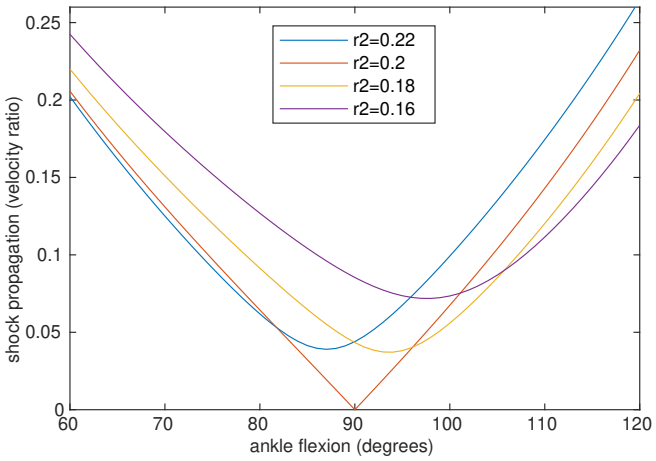

Fig. 3. Plots of shock propagation versus ankle angle for various values of r_2. The parameters are: $a_1 = 0.2\text{m}$, $b_1 = 0.05\text{m}$, $m_1 = 2\text{kg}$, $r_1 = 0.1\text{m}$, $a_2 = 0.25\text{m}$, $b_2 = 0.16\text{m}$ and $m_2 = 4\text{kg}$. The upper leg is modelled as a 0.4m, 5kg uniform thin rod oriented straight up; the knee is directly above the contact point; and the shock is the worst-case propagation of a step change in velocity from the ground contact point in the foot to the upper leg point at the knee, expressed as a velocity ratio.

upper leg and torso, respectively. In principle, the idea can be extended to 3D, in which case one would need three bats at right angles: one for each component of the impulse.

An important detail to bear in mind is that because no component of impulse propagates past the knee, the dynamics of the rest of the robot is irrelevant. Thus, the knee joint can have any angle, the upper leg any kinematic and inertia parameters, and the rest of the robot can have any number of other limbs in any state of contact with the environment at the time the foot hits the ground.

The challenge, in designing a leg to work like this, is to make the inertia parameters satisfy (3). For the foot, this requires that some mass be present to the rear of the ankle joint. This can be accomplished by making the foot extend backwards from the ankle as well as forwards, as shown in Figure 2. For the lower leg, some mass must be present above the knee. This has been illustrated in Figure 2 by extending the lower leg past the knee (the part marked 'extension' in the diagram). This would be a good place to put a knee guard or an actuator. If there is nothing functional to put here then one must resort to adding a small amount of dead weight.

Apart from the possibility of a small increase in leg mass, there is nothing in this design that reduces a legged robot's speed or maneuverability. Even the ankle angle can be adjusted according to need. If shock minimization is a priority then the robot can choose an ankle angle close to 90° on landing; and if it is not a priority then the robot can do something else. Likewise, if it is not feasible to design a leg that satisfies (3) exactly, then one can aim instead to minimize $|a_i b_i - r_i^2|$ subject to other design constraints. Such a design will not reduce shock propagation all the way to zero, but it will still be better than one that does not try to minimize these quantities.

To investigate the performance of this design, a numerical experiment was carried out on a 3-link leg considered in isolation (i.e., no torso) in which the objective was to find out how the shock propagation is affected by variation in the ankle angle and the value of r_2. The results are plotted in Figure 3, and the fixed parameter values are stated in the caption. The quantity plotted is the largest singular value of the matrix $\boldsymbol{R}$ described in the next section. It measures the worst-case propagation of shock from the ground contact point to a point in the upper leg at the knee, expressed as a ratio of two velocity magnitudes. For example, if the ratio is 0.2 then it means that there exists at least one direction in which a step change in foot velocity of 1m/s at the contact point causes a step change at the knee of 0.2m/s, generally in a different direction.

The decision to vary the ankle angle was prompted by concerns that 'fixing' it at 90° might be too restrictive; and the decision to vary r_2 was prompted by our opinion that getting r_2 to satisfy (3) in a practical leg design might be more difficult than r_1. The correct value for r_2 in this design is 0.2m, but a practical value is likely to be a little smaller, so we investigated two smaller values and only one larger one. The value $r_2 = 0.22\text{m}$ would require a substantial extension of the lower leg, and is likely to be impractical (unless it houses a bulky actuator); but a value of 0.16m is easily achievable with little or no extension.

One obvious conclusion that can be drawn from Figure 3 is that 90° is a good choice of angle regardless of inertia parameter values. Flexion angles greater than 90° place the heel closer to the ground at the moment of impact, which increases the chance that the heel will hit the ground before the impact has been fully absorbed; whereas angles less than 90° result in greater shock propagation.

A second conclusion is that if $r_2^2 < a_2 b_2$ in some proposed design then even a small increase in r_2 will improve the shock propagation properties of the leg at all ankle flexion angles less than, equal to and slightly greater than 90°.

V. A General Formula

This section derives the formula for the matrix that maps a step change in the velocity of the ground-contact point in the foot to the consequential step change in velocity of a chosen point in the torso. Possible choices for the latter include the torso's CoM, the position of the inertial measurement unit, and the rotation centre of the hip joint. This matrix can be used in various ways to measure the shock propagation properties of a leg design. For example, the largest singular value provides a measure of worst-case transmission of shock from the foot to the chosen point in the torso.

This section uses both spatial and 3-D Euclidean vectors. To avoid confusion, the latter are marked with an arrow. Thus, $\boldsymbol{v}_i$ denotes the spatial velocity of body i, whereas $\vec{\boldsymbol{v}}_P$ denotes the Euclidean velocity of a body-fixed point located at P. (Remember that 'velocity' means 'step change in velocity'.) In the equations below, it is assumed that all quantities are expressed in coordinates based on a single common Cartesian coordinate frame.

Figure 4 shows a general robot leg consisting of a chain of rigid bodies numbered 1 to n connected together by joints

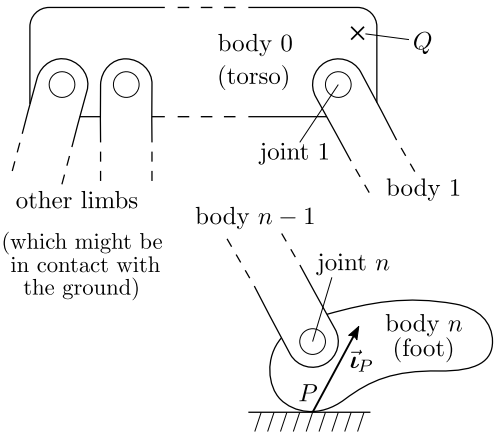

Fig. 4. A general robot leg, modelled as a chain of rigid bodies, in which the foot has struck the ground at point P.

also numbered 1 to n. Body n is the foot; and this body strikes the ground at point P, causing a ground-reaction impulse of $\vec{\imath}_P$, which in turn causes a velocity of $\vec{\boldsymbol{v}}_P$ in the body-fixed point at P. Body 0 is the torso, and Q is a point of interest in the torso that may be chosen freely by the user, which acquires a velocity of $\vec{\boldsymbol{v}}_Q$ as a consequence of the foot striking the ground. The objective of this section is to obtain a formula for the 3×3 matrix $\boldsymbol{R}$ that maps $\vec{\boldsymbol{v}}_P$ to $\vec{\boldsymbol{v}}_Q$ according to

$$\vec{\boldsymbol{v}}_Q = \boldsymbol{R}\vec{\boldsymbol{v}}_P \,. \tag{4}$$

The closer $\boldsymbol{R}$ is to zero, the less shock is felt at Q. By defining $\boldsymbol{R}$ to be a mapping between Euclidean velocity vectors, we avoid any difficulties associated with physical dimensions and choice of units.

The torso is characterized by its articulated-body inertia, $\boldsymbol{I}_0^A$, which includes the inertial effects of the rest of the robot; that is, every part of the robot except the leg containing bodies 1 to n. If there are other limbs in the rest of the robot that make contact with the ground, or other fixed parts of the environment, then $\boldsymbol{I}_0^A$ includes also the effects of the kinematic constraints on these other limbs, subject to the assumption that these constraints do not change as a consequence of the impact.

If there are at least two other limbs making contact with the environment then there will be at least one kinematic loop in the rest of the robot. For this reason, it is probably best to calculate $\boldsymbol{I}_0^A$ via the projection method [9], which proceeds as follows. First, let $\dot{\boldsymbol{q}}$ be the joint-space velocity vector for the rest of the robot. This vector includes six variables that describe the velocity of the torso, which is treated as the floating base. Next, let $\boldsymbol{J}$ be the Jacobian that maps $\dot{\boldsymbol{q}}$ to $\boldsymbol{v}_0$ (torso velocity) according to

$$\boldsymbol{v}_0 = \boldsymbol{J}\dot{\boldsymbol{q}} \,.$$

Obtaining $\boldsymbol{J}$ is easy because $\dot{\boldsymbol{q}}$ already contains the six variables that define $\boldsymbol{v}_0$, and the other variables have no effect. Next, let the kinematic constraints on $\dot{\boldsymbol{q}}$ be given by

$$\boldsymbol{K}\dot{\boldsymbol{q}} = \boldsymbol{0} \,.$$

This equation can be solved to express $\dot{\boldsymbol{q}}$ in the form

$$\dot{\boldsymbol{q}} = \boldsymbol{G}\,\dot{\boldsymbol{y}} \,,$$

where $\dot{\boldsymbol{y}}$ is a subvector of $\dot{\boldsymbol{q}}$ containing any maximal set of independent velocity variables, and $\boldsymbol{G}$ is a full-rank matrix that spans the null space of $\boldsymbol{K}$ (so $\boldsymbol{K}\boldsymbol{G} = \boldsymbol{0}$). Finally, let $\boldsymbol{H}$ be the joint-space inertia matrix of the rest of the robot. Given $\boldsymbol{J}$, $\boldsymbol{G}$ and $\boldsymbol{H}$, the formula for $\boldsymbol{I}_0^A$ is

$$\boldsymbol{I}_0^A = (\boldsymbol{J}\boldsymbol{G}(\boldsymbol{G}^{\mathrm{T}}\boldsymbol{H}\boldsymbol{G})^{-1}\boldsymbol{G}^{\mathrm{T}}\boldsymbol{J}^{\mathrm{T}})^{-1} \,. \tag{5}$$

(This is equation 7.12 in [9] with $\boldsymbol{J}\boldsymbol{G}$ in place of $\boldsymbol{J}$ and $\boldsymbol{G}^{\mathrm{T}}\boldsymbol{H}\boldsymbol{G}$ in place of $\boldsymbol{H}$. See also [9, §3.2] for more details about $\boldsymbol{G}$.) The inner inversion in (5) is always possible because $\boldsymbol{H}$ is positive definite and $\boldsymbol{G}$ has full rank. However, the outer inversion requires that the torso have a full six degrees of motion freedom.

Having captured all relevant dynamics of the rest of the robot in $\boldsymbol{I}_0^A$, we now turn our attention to the leg. Each body i in the leg is characterized by its rigid-body inertia, $\boldsymbol{I}_i$, from which can be calculated its articulated-body inertia, $\boldsymbol{I}_i^A$, which takes into account the inertial effects of the bodies between body i and the torso, plus the effects included in $\boldsymbol{I}_0^A$. Formulae for calculating articulated-body inertias are given in (21) and (26) in the appendix.

To calculate $\boldsymbol{R}$, the first step is to work out the spatial velocity of the foot, $\boldsymbol{v}_n$, caused by its collision with the ground. To do this, we use the following equations:

$$\boldsymbol{\iota}_n \;=\; \boldsymbol{I}_n^A\boldsymbol{v}_n \,, \tag{6}$$

$$\vec{\boldsymbol{v}}_P \;=\; \boldsymbol{P}\boldsymbol{v}_n \,, \tag{7}$$

$$\boldsymbol{\iota}_n \;=\; \boldsymbol{P}^{\mathrm{T}}\vec{\boldsymbol{\iota}}_P \,, \tag{8}$$

where (6) is the articulated-body impulsive equation of motion of the foot, and $\boldsymbol{P}$ is the matrix that maps the spatial velocity of a rigid body to the linear velocity of the body-fixed point at P. Its value is

$$\boldsymbol{P} = \begin{bmatrix} 0 & P_z & -P_y & 1 & 0 & 0 \\ -P_z & 0 & P_x & 0 & 1 & 0 \\ P_y & -P_x & 0 & 0 & 0 & 1 \end{bmatrix} , \tag{9}$$

where P_x, etc., are the coordinates of P. As can be seen from (8), $\boldsymbol{P}$ has the additional property that $\boldsymbol{P}^{\mathrm{T}}$ maps a Euclidean impulse vector representing an impulse having a line of action passing through P to the equivalent spatial vector. Later on, we will also need the matrix $\boldsymbol{Q}$, analogous to $\boldsymbol{P}$, for use with the point Q.

Given (6)–(8), the calculation of $\boldsymbol{v}_n$ from $\vec{\boldsymbol{v}}_P$ proceeds as follows:

$$\vec{\boldsymbol{v}}_P = \boldsymbol{P}\boldsymbol{v}_n = \boldsymbol{P}(\boldsymbol{I}_n^A)^{-1}\boldsymbol{\iota}_n = \boldsymbol{P}(\boldsymbol{I}_n^A)^{-1}\boldsymbol{P}^{\mathrm{T}}\vec{\boldsymbol{\iota}}_P \,,$$

which implies

$$\vec{\boldsymbol{\iota}}_P = (\boldsymbol{P}(\boldsymbol{I}_n^A)^{-1}\boldsymbol{P}^{\mathrm{T}})^{-1}\vec{\boldsymbol{v}}_P \,. \tag{10}$$

Combining (6), (8) and (10) gives

$$\begin{aligned} \boldsymbol{v}_n \;&=\; (\boldsymbol{I}_n^A)^{-1}\boldsymbol{\iota}_n = (\boldsymbol{I}_n^A)^{-1}\boldsymbol{P}^{\mathrm{T}}\vec{\boldsymbol{\iota}}_P \\ &=\; (\boldsymbol{I}_n^A)^{-1}\boldsymbol{P}^{\mathrm{T}}(\boldsymbol{P}(\boldsymbol{I}_n^A)^{-1}\boldsymbol{P}^{\mathrm{T}})^{-1}\vec{\boldsymbol{v}}_P \,. \end{aligned}$$

So we have

$$\boldsymbol{v}_n = \boldsymbol{B}\vec{\boldsymbol{v}}_P\,, \tag{11}$$

where

$$\boldsymbol{B} = (\boldsymbol{I}_n^A)^{-1}\boldsymbol{P}^{\mathrm{T}}(\boldsymbol{P}(\boldsymbol{I}_n^A)^{-1}\boldsymbol{P}^{\mathrm{T}})^{-1}\,. \tag{12}$$

The next step is to calculate $\boldsymbol{v}_0$ from $\boldsymbol{v}_n$. To do this we use an acceleration propagator, $\boldsymbol{A}$, defined as follows:

$$\boldsymbol{A} = \boldsymbol{A}_1\boldsymbol{A}_2\cdots\boldsymbol{A}_n\,, \tag{13}$$

where $\boldsymbol{A}_i$ is the acceleration propagator from body i to body $i-1$. As the name suggests, these matrices are normally used to propagate accelerations from one body to another, but in impulsive dynamics they serve to propagate changes in velocity. Acceleration propagators are not a new idea, and examples can be found in [7], [8]. Formulae for calculating acceleration propagators are given in the appendix. The calculation of $\boldsymbol{v}_0$ is accomplished by

$$\boldsymbol{v}_0 = \boldsymbol{A}\boldsymbol{v}_n\,. \tag{14}$$

The final step is to calculate $\vec{\boldsymbol{v}}_Q$ from $\boldsymbol{v}_0$, which is accomplished using the matrix $\boldsymbol{Q}$ mentioned earlier. Putting everything together, we have

$$\vec{\boldsymbol{v}}_Q = \boldsymbol{Q}\boldsymbol{A}\boldsymbol{B}\vec{\boldsymbol{v}}_P\,, \tag{15}$$

hence

$$\boldsymbol{R} = \boldsymbol{Q}\boldsymbol{A}\boldsymbol{B}\,. \tag{16}$$

The analysis presented here relies on formulae given in the appendix, which in turn rely on assumptions about the impulsive behaviour of the actuators. Apart from that, the only assumptions are that the foot strikes the ground at a single point, or an area small enough to be regarded as a single point, and that the dynamics of shock propagation in a robot leg can be modelled adequately as an impulse in a rigid-body system.

A. *Effect of Rotor Inertia*

Equation (16) allows for general kinematic and inertia parameters, as well as a general state of contact between other limbs and the ground at the time of impact. However, it also allows for actuators that generate an impulse in reaction to a step change in joint velocity, thanks to the formulae in the Appendix (Case 2). So it would be interesting to see what effect this kind of actuator has on shock propagation up the leg. To this end, Figure 5 shows two graphs that repeat the curve of the ideal design in Figure 3, and add several more curves in which either the ankle joint or the knee joint is actuated by an electric motor having a rotor inertia of $10^{-4}\mathrm{kgm}^2$ which is connected to the joint via a perfect reduction gear with a ratio of 10, 15 or 20:1. A perfect gear is a rigid transmission, so a step change in joint velocity implies a step change in rotor velocity, which requires an impulse. Negative gear ratios were also tried, but their effect differs only slightly from that of the corresponding positive gear ratio.

The top graph shows that an actuator of this kind at the ankle increases shock propagation at all ankle flexion angles

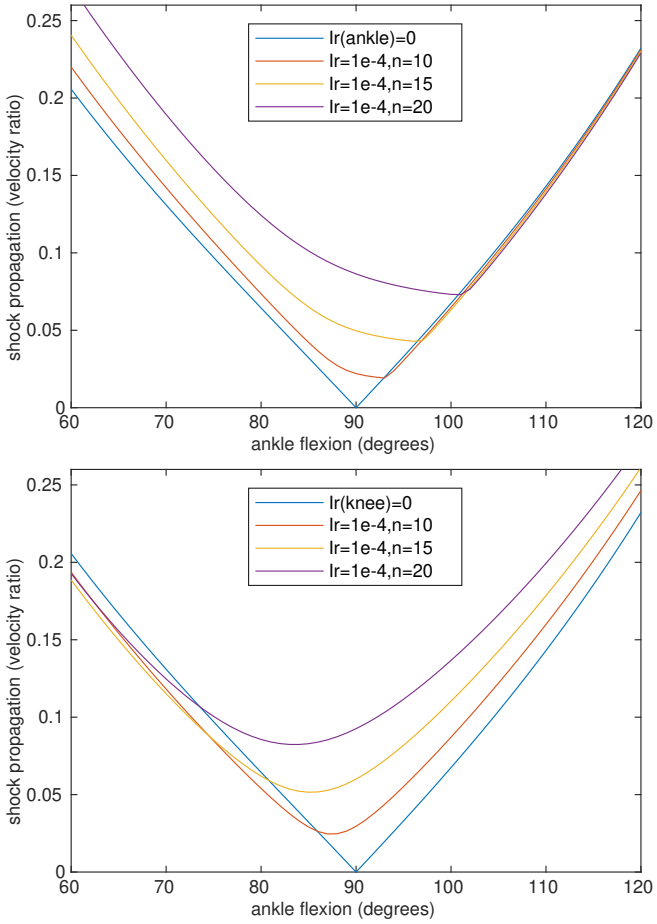

Fig. 5. Plots of shock propagation versus ankle angle for various values of ankle (top graph) and knee (bottom graph) rotor inertia and gear ratio, for the same leg design as in Figure 3 ($r_2 = 0.2\mathrm{m}$)

less than a threshold which is greater than $90°$; while the bottom graph shows that an actuator at the knee increases shock propagation at all angles above a threshold below $90°$, but also reduces it slightly at angles below the threshold. Legs with actuators at both joints were also investigated, and the effect of the two actuators together is approximately the sum of their individual effects.

Graphs like these show us that the overall effect of actuators that generate an impulse in response to a step change in joint velocity is to increase shock propagation up the leg, although the details vary with joint angle. This is a good argument in favour of including at least a small amount of elasticity in the transmission. It also shows that the mass distribution technique described in this paper is best used in combination with other shock-reduction measures.

VI. Conclusion

This paper has investigated how the mass distribution in a robot's leg affects shock propagation from the foot to the torso. An example was given of an 'ideal' leg that isolates the torso completely from all shocks arising from in-plane ground-reaction forces at the foot; and a formula was presented for a shock propagation matrix that can be used to

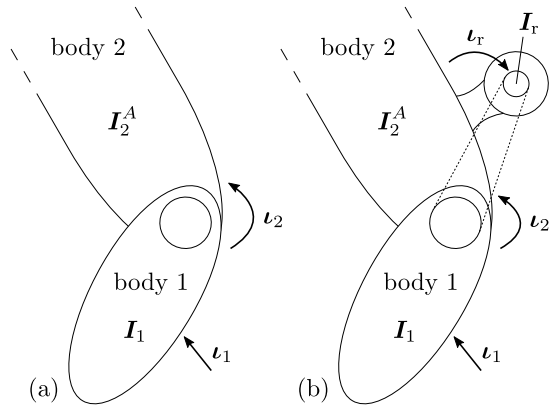

Fig. 6. Calculation of acceleration propagators (a) without and (b) with inertial effect of the actuator.

quantify the shock propagation in any given leg design. Both are believed to be new. A few graphs were presented showing how shock propagation varies with mass distribution, ankle flexion angle and actuator behaviour during impact. One obvious use for a shock propagation matrix would be design optimization studies aimed at reducing the shock experienced in the torso. The problem of shock reduction is likely to become more important as legged robots reach higher speeds, and this paper provides one more tool to help mitigate this problem.

APPENDIX

This appendix presents formulae for articulated-body inertias and acceleration propagators under two different assumptions about how the actuator behaves during impulsive dynamics. The first is the assumption that the actuator does not produce an impulse. This assumption is valid if the actuator is a direct-drive motor, or if there is a series elastic element between the actuator and the joint. The second is the assumption that the actuator produces an inertial impulse only. This assumption is valid if the actuator consists of a motor and a highly efficient gear, such as a cable drive, that can be regarded as perfect (i.e., no friction, compliance or backlash). The formulae obtained under the first assumption exist already in the literature, but those obtained under the second assumption appear to be new. As mentioned in Section III, 'velocity' means 'step change in velocity' in the text below. All quantities are expressed in a common coordinate system that can be chosen freely by the user.

If the robot has other limbs in contact with the environment at the time of the impact then it is assumed that the impulse does not alter the state of these other contacts. This assumption allows existing contacts to be treated as equality constraints for the purpose of calculating articulated-body inertias.

Case 1: no actuator impulse

Referring to Figure 6(a), an impulse $\boldsymbol{\iota}_1$ acts on body 1, which has inertia $\boldsymbol{I}_1$, giving it a velocity of $\boldsymbol{v}_1$ and causing an impulse $\boldsymbol{\iota}_2$ to be transmitted across the connecting joint to body 2, giving it a velocity of $\boldsymbol{v}_2$. As body 2 might have other bodies connected to it, it is characterized by its articulated-body inertia, $\boldsymbol{I}_2^A$. Although not strictly necessary, we shall assume that the joint has only one degree of motion freedom, and can therefore be characterized by a vector, $\boldsymbol{s}$, such that the relative velocity of the two bodies is a scalar multiple of $\boldsymbol{s}$. (For a revolute joint, $\boldsymbol{s}$ is the joint axis vector.) The relevant equations are

$$\begin{aligned} \boldsymbol{\iota}_1 - \boldsymbol{\iota}_2 &= \boldsymbol{I}_1 \boldsymbol{v}_1 & \boldsymbol{v}_2 &= \boldsymbol{v}_1 + \boldsymbol{s}\alpha \\ \boldsymbol{\iota}_2 &= \boldsymbol{I}_2^A \boldsymbol{v}_2 & \boldsymbol{s}^\mathrm{T}\boldsymbol{\iota}_2 &= 0\,. \end{aligned} \tag{17}$$

The ones on the left are equations of motion, while those on the right describe the constraint imposed by the joint and the fact that constraint impulses do no work. These equations can be solved for α as follows:

$$\boldsymbol{s}^\mathrm{T}\boldsymbol{I}_2^A(\boldsymbol{v}_1 + \boldsymbol{s}\alpha) = 0 \quad \Rightarrow \quad \alpha = -\frac{\boldsymbol{s}^\mathrm{T}\boldsymbol{I}_2^A\boldsymbol{v}_1}{\boldsymbol{s}^\mathrm{T}\boldsymbol{I}_2^A\boldsymbol{s}}\,, \tag{18}$$

which implies

$$\boldsymbol{v}_2 = \boldsymbol{v}_1 - \frac{\boldsymbol{s}\boldsymbol{s}^\mathrm{T}\boldsymbol{I}_2^A\boldsymbol{v}_1}{\boldsymbol{s}^\mathrm{T}\boldsymbol{I}_2^A\boldsymbol{s}}\,. \tag{19}$$

If we define the acceleration propagator, $\boldsymbol{A}$, to be the matrix that maps $\boldsymbol{v}_1$ to $\boldsymbol{v}_2$ according to $\boldsymbol{v}_2 = \boldsymbol{A}\boldsymbol{v}_1$ then

$$\boldsymbol{A} = \mathbf{1} - \frac{\boldsymbol{s}\boldsymbol{s}^\mathrm{T}\boldsymbol{I}_2^A}{\boldsymbol{s}^\mathrm{T}\boldsymbol{I}_2^A\boldsymbol{s}}\,. \tag{20}$$

(A bold $\mathbf{1}$ denotes an identity matrix.) Given $\boldsymbol{A}$, the articulated-body inertia of body 1 can be expressed as

$$\boldsymbol{I}_1^A = \boldsymbol{I}_1 + \boldsymbol{I}_2^A\boldsymbol{A}\,. \tag{21}$$

This can be verified by checking that $\boldsymbol{\iota}_1 = \boldsymbol{I}_1^A\boldsymbol{v}_1$.

Case 2: inertial actuator impulse

Figure 6(b) shows a modification of the situation in Figure 6(a) in which a motor is embedded in body 2 and drives the joint via a gear with gear ratio n defined as follows: if the rotor rotates by an angle θ about $\boldsymbol{s}_\mathrm{r}$ (the rotation axis of the rotor) relative to body 2 then body 1 rotates by an angle θ/n about $\boldsymbol{s}$ (the rotation axis of the joint) relative to body 2. The relevant equations are now

$$\begin{aligned} \boldsymbol{\iota}_1 - \boldsymbol{\iota}_2 &= \boldsymbol{I}_1 \boldsymbol{v}_1 & \boldsymbol{v}_2 &= \boldsymbol{v}_1 + \boldsymbol{s}\alpha \\ \boldsymbol{\iota}_2 - \boldsymbol{\iota}_\mathrm{r} &= \boldsymbol{I}_2^A \boldsymbol{v}_2 & \boldsymbol{v}_\mathrm{r} &= \boldsymbol{v}_2 - n\boldsymbol{s}_\mathrm{r}\alpha \\ \boldsymbol{\iota}_\mathrm{r} &= \boldsymbol{I}_\mathrm{r}\boldsymbol{v}_\mathrm{r} & \boldsymbol{s}^\mathrm{T}\boldsymbol{\iota}_2 &= n\boldsymbol{s}_\mathrm{r}^\mathrm{T}\boldsymbol{\iota}_\mathrm{r}\,. \end{aligned} \tag{22}$$

The ones on the left are equations of motion, and those on the right describe the motion freedoms allowed by the two joints and the assumption that the gear is perfect (power in equals power out). The minus sign in $\boldsymbol{v}_2 - n\boldsymbol{s}_\mathrm{r}\alpha$ is there because $\boldsymbol{s}\alpha$ is the velocity of body 2 relative to body 1, which is the opposite of the sense used to define n. These equations can be solved for α as follows:

$$\begin{aligned} 0 &= \boldsymbol{s}^\mathrm{T}\boldsymbol{\iota}_2 - n\boldsymbol{s}_\mathrm{r}^\mathrm{T}\boldsymbol{\iota}_\mathrm{r} \\ &= \boldsymbol{s}^\mathrm{T}\boldsymbol{I}_2^A\boldsymbol{v}_2 + (\boldsymbol{s} - n\boldsymbol{s}_\mathrm{r})^\mathrm{T}\boldsymbol{\iota}_\mathrm{r} \\ &= \boldsymbol{s}^\mathrm{T}\boldsymbol{I}_2^A(\boldsymbol{v}_1 + \boldsymbol{s}\alpha) + (\boldsymbol{s} - n\boldsymbol{s}_\mathrm{r})^\mathrm{T}\boldsymbol{I}_\mathrm{r}\boldsymbol{v}_\mathrm{r} \\ &= \boldsymbol{s}^\mathrm{T}\boldsymbol{I}_2^A(\boldsymbol{v}_1 + \boldsymbol{s}\alpha) + (\boldsymbol{s} - n\boldsymbol{s}_\mathrm{r})^\mathrm{T}\boldsymbol{I}_\mathrm{r}(\boldsymbol{v}_1 + (\boldsymbol{s} - n\boldsymbol{s}_\mathrm{r})\alpha)\,, \end{aligned}$$

which implies

$$\alpha = \boldsymbol{e}^{\mathrm{T}} \boldsymbol{v}_1 \tag{23}$$

where

$$\boldsymbol{e}^{\mathrm{T}} = -\frac{\boldsymbol{s}^{\mathrm{T}} \boldsymbol{I}_2^A + (\boldsymbol{s} - n\boldsymbol{s}_{\mathrm{r}})^{\mathrm{T}} \boldsymbol{I}_{\mathrm{r}}}{\boldsymbol{s}^{\mathrm{T}} \boldsymbol{I}_2^A \boldsymbol{s} + (\boldsymbol{s} - n\boldsymbol{s}_{\mathrm{r}})^{\mathrm{T}} \boldsymbol{I}_{\mathrm{r}} (\boldsymbol{s} - n\boldsymbol{s}_{\mathrm{r}})} \,. \tag{24}$$

The acceleration propagator matrix is then

$$\boldsymbol{A} = \boldsymbol{1} + \boldsymbol{s}\boldsymbol{e}^{\mathrm{T}} \,. \tag{25}$$

Observe that this equation agrees with (20) when $n = 1$ and $\boldsymbol{s}_{\mathrm{r}} = \boldsymbol{s}$, which is the case that corresponds to direct drive. Given $\boldsymbol{e}$ and $\boldsymbol{A}$, the formula for the articulated-body inertia of body 1 is

$$\boldsymbol{I}_1^A = \boldsymbol{I}_1 + \boldsymbol{I}_{\mathrm{r}} + \boldsymbol{I}_2^A \boldsymbol{A} + \boldsymbol{I}_{\mathrm{r}} (\boldsymbol{s} - n\boldsymbol{s}_{\mathrm{r}}) \boldsymbol{e}^{\mathrm{T}} \,. \tag{26}$$

This equation agrees with (21) when $n = 1$ and $\boldsymbol{s} = \boldsymbol{s}_{\mathrm{r}}$ if one takes into account that $\boldsymbol{I}_1$ in (21) would include the rotor's inertia if the joint were being directly driven, and would therefore be equal to $\boldsymbol{I}_1 + \boldsymbol{I}_{\mathrm{r}}$ in (26).

REFERENCES

[1] R. Alexander, "Three Uses for Springs in Legged Locomotion", *Int. J. Robotics Research*, vol. 9, no. 2, pp. 53–61, 1990.

[2] R. Bartlett, *Introduction to Sports Biomechanics: Analysing Human Movement Patterns, Second Edition*, New York: Routledge (Taylor and Francis Group), 2007.

[3] J. Bingham, J. Lee, R. Haksar, J. Ueda and C. Liu, "Orienting in Mid-air through Configuration Changes to Achieve a Rolling Landing for Reducing Impact after a Fall", Proc. IEEE Int. Conf. Intelligent Robots and Systems, 2014, pp. 3610–3617.

[4] O. Bruneau, F. B. Ouezdou, and J. G. Fontaine, "Dynamic Walk of a Bipedal Robot Having Flexible Feet", Proc. IEEE Int. Conf. Intelligent Robots and Systems, 2001, pp. 512–517.

[5] W. Choi, H. Dallali, G. Medrano-Cerda, N. Tsagarakis and D. Caldwell, "How Leg Compliance and Posture affects Impact Forces during Landing", Proc. IEEE Int. Conf. Robotics and Biomimetics, 2014, pp. 961–967.

[6] H. Dallali, P. Kormushev, N. Tsagarakis and D. Caldwell, "Can Active Impedance Protect Robots from Landing Impact?", Proc. IEEE-RAS Int. Conf. Humanoid Robots, 2014, pp. 1022–1027.

[7] R. Featherstone, *Robot Dynamics Algorithms*, Ph.D. thesis, Dept. Artificial Intelligence, University of Edinburgh, 1984.

[8] R. Featherstone, *Robot Dynamics Algorithms*, Boston/Dordrecht/Lancaster: Kluwer Academic Publishers, 1987.

[9] R. Featherstone, *Rigid Body Dynamics Algorithms*, New York: Springer, 2008.

[10] C. Glocker, "An Introduction to Impacts", in: *Nonsmooth Mechanics of Solids*, eds. J. Haslinger and G. E. Stavroulakis, pp. 45–101, Springer, 2006.

[11] K. Hashimoto, A. Hayashi, T. Sawato, Y. Yoshimura, T. Asano, and K. Hattori, "Terrain-Adaptive Control to Reduce Landing Impact Force for Human-Carrying Biped Robot", Proc. IEEE/ASME Conf. Advanced Intelligent Mechatronics, 2009, pp. 174–179.

[12] S. Hauser, P. Eckert, A. Tuleu and A. Ijspeert, "Friction and damping of a compliant foot based on granular jamming for legged robots", Proc. IEEE RAS/EMBS Int. Conf. Biomedical Robotics and Biomechatronics, 2016, pp. 1160–1165.

[13] H. Ishihara, T. Nagayama, H. Tomori, and T. Nakamura, "Landing Method for a one-legged robot with artificial muscles and an MR brake", 41st Annual Conf. IEEE Ind. Elec. Society, IECON 2015, pp. 1879–1884.

[14] Y. Kim, B. Lee, J. Yoo, J. Kim, and J. Ryu, "Compensation for the Landing Impact Force of a Humanoid Robot by Time Domain Passivity Approach", Proc. IEEE Int. Conf. Robotics and Automation, 2006, pp. 1225–1230.

[15] S. Kwon and J. Park, "Kinesiology-Based Robot Foot Design for Human-Like Walking", *Int. J. Advanced Robotic Systems*, vol. 9, pp. 259–269, 2012.

[16] D. N. Nenchev and K. Yoshida, "Impact Analysis and Post-Impact Motion Control Issues of a Free-Floating Space Robot Subject to a Force Impulse", *IEEE Trans. Robotics and Automation*, vol. 15, no. 3, pp. 548–557, 1999.

[17] F. B. Ouezdou, S. Alfayad and B. Almasri, "Comparison of Several Kinds of Feet for Humanoid Robot", Proc. IEEE-RAS Int. Conf. Humanoid Robots, 2005, pp. 123–128.

[18] J. H. Park and H. Chung, "Impedance Control and Modulation for Stable Footing in Locomotion of Biped Robots", Proc. IEEE Int. Conf. Intelligent Robots and Systems, 1999, pp. 1786–1791.

[19] K. Radkhak and O. Stryk, "A study of the passive rebound behavior of bipedal robots with stiff and different types of elastic actuation", Proc. IEEE Int. Conf. Robotics and Automation, 2014, pp. 5095–5102.

[20] M. H. Raibert, *Legged robots that balance*, Cambridge: MIT Press, 1986.

[21] P. G. Santos, E. Garcia and J. Estremera, "Improving walking-robot performances by optimizing leg distribution", *Autonomous Robots*, vol. 23, pp. 247–258, 2007.

[22] Y. Sato, E. Ohashi and K. Ohnishi, "Impact Force reduction for hopping robot", Proc. 31st Annual Conf. IEEE Ind. Elec. Society, IECON 2005, pp. 1821–1826.

[23] E. Schumann, N. Smit-Anseeuw, P. Zaytsev, R. Gleason, K. Shorter, and C. Remy, "Effects of Foot Stiffness and Damping on Walking Robot Performance", Proc. IEEE Int. Conf. Robotics and Automation, 2019, pp. 3698–3704.

[24] I. D. Walker, "Impact Configurations and Measures for Kinematically Redundant and Multiple Armed Robot Systems", *IEEE Trans. Robotics and Automation*, vol. 10, no. 5, pp. 670–683, 1994.

[25] X. Wan, T. Urakubo and Y. Tada, "Landing Motion of a Legged Robot with Impact Force Reduction and Joint Torque Minimization", Proc. Second Int. Conf. Robot, Vision and Signal Processing, 2013, pp. 259–264.

[26] Jin'ichi Yamaguchi, Atsuo Takanishi and Ichiro Kato, "Experimental Development of a Foot Mechanism with Shock Absorbing Material for Acquisition of Landing Surface Position Information and Stabilization of Dynamic Biped Walking", Proc. IEEE Int. Conf. Robotics and Automation, 1995, pp. 2892–2899.